CORE
Metadata, citation and similar papers at core.ac.uk
Provided by Sheffield Hallam University Research Archive

Sheffield
Hallam University

SHARPENS YOUR THINKING

Optical and electrical activity of defects in rare earth implanted Si

EVANS-FREEMAN, J. H. and VERNON-PARRY, K.

Available from Sheffield Hallam University Research Archive (SHURA) at:

http://shura.shu.ac.uk/984/

This document is the author deposited version. You are advised to consult the publisher's version if you wish to cite from it.

Published version

EVANS-FREEMAN, J. H. and VERNON-PARRY, K. (2005). Optical and electrical activity of defects in rare earth implanted Si. Optical materials.

Repository use policy

Copyright © and Moral Rights for the papers on this site are retained by the individual authors and/or other copyright owners. Users may download and/or print one copy of any article(s) in SHURA to facilitate their private study or for non-commercial research. You may not engage in further distribution of the material or use it for any profit-making activities or any commercial gain.

Sheffield Hallam University Research Archive
http://shura.shu.ac.uk

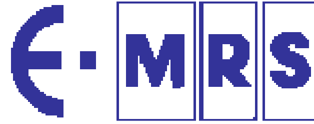

Strasbourg (France)

MANUSCRIPT COVER PAGE FORM

E-MRS Symposium : C, Rare Earth Doped Photonic Materials

Paper Number : C-XI.01

Title of Paper : Optical and Electrical Activity of Defects in Rare Earth Implanted Si

Corresponding author : Professor J Evans-Freeman

Full mailing address : Materials and Engineering Research Institute
ACES Faculty
Sheffield Hallam University
Howard Street
Sheffield S1 1WB
United Kingdom

Telephone : 0114 225 4037
Fax : 0114 225 3500
Email : j.evans-freeman@shu.ac.uk

Optical and Electrical Activity of Defects in Rare Earth Implanted Si

J H Evans-Freeman and K D Vernon-Parry

Materials and Engineering Research Institute
Sheffield Hallam University
Sheffield
S1 1WB
United Kingdom

A common technique for introducing rare earth atoms into Si and related materials for photonic applications is ion implantation. It is compatible with standard Si processing, and also allows high, non-equilibrium concentrations of rare earths to be introduced. However, the high energies often employed mean that there are collision cascades and potentially severe end-of-range damage. This paper reports on studies of this damage, and the competition it may present to the optical activity of the rare earths. Er-, Si, and Yb-implanted Si samples have been investigated, before and after anneals designed to restore the sample crystallinity. The electrical activity of defects in as-implanted Er, Si, and Yb doped Si has been studied by Deep Level Transient Spectroscopy (DTLS) and the related, high resolution technique, Laplace DLTS (LDLTS), as a function of annealing. Er-implanted Si, regrown by solid phase epitaxy at 600degrees C and then subject to a rapid thermal anneal, has also been studied by time-resolved photoluminescence (PL). The LDLTS studies reveal that there are clear differences in the defect population as a function of depth from the surface, and this is attributed to different defects in the vacancy-rich and interstitial-rich regions. Defects in the interstitial-rich region have electrical characteristics typical of small extended defects, and these may provide the precursors for larger structural defects in annealed layers. The time-resolved PL of the annealed layers, in combination with electron microscopy, shows that the Er emission at 1.54microns contains a fast component attributed to non-radiative recombination at deep states due to small dislocations. It is

concluded that there can be measurable competition to the radiative efficiency in rare-earth implanted Si that is due to the implantation and is not specific to Er.

Introduction

If a light emitter based on rare earth emission in Si as a host is to be realised, ion implantation would be a favoured incorporation route. It allows for high (non-equilibrium) concentrations of the ions to be incorporated, an essential prerequisite for usable output powers. Er-doped Si nanocrystal co-doped SiO_2 [1] is currently a strong contender for fabrication of a Si laser, since it was reported that Er can be excited indirectly in such a system [2,3]. Despite the excellent promise of this system [1], there is still the considerable advantage that ion-implantation of Er into Si is compatible with VLSI processing, and efforts continue to overcome fundamental problems, such as temperature-dependent quenching of the photoluminescence (PL) signal, for example, by band gap engineering using SiGe. [4]

One of the underlying problems of using rare earth emission in Si as a host is the relative lifetimes of various parallel processes. The radiative lifetime of the Er can be many milliseconds in an insulator and is reduced by faster non-radiative recombination in Si, an effect which is increasingly prevalent as the temperature rises. A further complication arises in ion implantation, as the implantation introduces defects which can be hard to remove. The microelectronics industry currently has issues with ion implantation damage being responsible for various processing bottlenecks, for example, the phenomenon of Transient Enhanced Diffusion (TED). [5] In TED, the implanted boron atoms diffuse away from their intended location, because their interstitial-assisted diffusion is enhanced by the interstitials created during implantation. If implant-related damage remains after an anneal, it is typically seen as end-of-range loops. Such loops are known to have associated electrical activity [6] and optical activity, [7] and therefore are of critical importance in device design and subsequent functionality. They are formed from an excess of interstitials which have been unable either to recombine with

vacancies or to escape to the surface during anneal. The optical activity can be observed as the well-known dislocation line D1 which happens to possess the same emission wavelength as Er. [7]

Electrical activity implies trapping or recombination through defect-related deep states, which will provide non-radiative competition to the inherently slower Er luminescence. This will be a problem if, for example, a p-n style vertical structure is to be used for the device, when these defects will be in the active area of the device. This paper presents a detailed study of ion-implant-related damage in rare earth implanted Si. We have examined the effects on the PL emission by time resolved PL measurements on annealed samples, and we have linked this to an electrical study of pre-anneal damage by high resolution Laplace Deep Level Transient Spectroscopy (LDLTS). The pre-anneal study was to ascertain whether pre-cursors to end-of-range loops could be detected electrically, as they have been predicted to exist in Si implanted with boron. [8]

Experimental Details

The time resolved PL measurements were carried out on layers which contained sufficient Er and O to yield a measurable PL signal. The oxygen was co-implanted because it has been reported to increase the intensity of the erbium-related luminescence and reduce the quenching of the luminescence at increased temperatures [9,10]. The electrical measurements were carried out on samples implanted with a low dose, because the high doses necessary for PL caused too much carrier removal, due to deep traps, for electrical techniques such as DLTS and capacitance-voltage (C-V) to be carried out before annealing.

The starting material for the PL decay measurements was p-type (100) Si with a background doping of $2x10^{16}$ cm^{-3}. It was given a multiple oxygen implant (doses of 3.2, 2, 1.4, 1.1, 5 and $1x10^{14}$ cm^{-2} at 450, 300, 200, 140, 90 and 70 keV respectively) and a single erbium implant with a dose of $5x10^{13}$ cm^{-2} at 1 MeV. This produced a uniform oxygen concentration of $1x10^{19}$ cm^{-3} to a depth of 0.9 μm, and a peak Er concentration of $3x10^{18}$ cm^{-3} at a depth of 0.3 μm as measured by SIMS. Electron backscattered diffraction (EBSD) pattern analysis revealed that these implants were not sufficient to cause amorphisation but lateral variations in dose produced slight differences in damage. From the SIMS and EBSD results we estimate that the dose variation across the wafer was <4%. A rapid thermal anneal (RTA) at 900°C for 60s annealed out point defects caused by the implants, and was sufficient for observation of strong erbium-related luminescence from the sample. The sample was mounted in a variable temperature closed-cycle helium cryostat and excited by 514.2 nm radiation from an Ar ion laser. For the PL decay measurements, the laser light was modulated with an acousto-optic modulator to produce pulses of 5ms duration with a repetition rate of 83Hz. The signal was passed through a notch filter centred on 1.536 ± 0.014 μm and was detected by a fast North Coast Germanium detector cooled to 77K, and the decaying signal was collected using a Windows-based transient acquisition card. The overall response time of the system was measured in two ways. Firstly, the notch filter was removed from the system, and the decay of the laser light scattered from the sample mount was recorded. Secondly, the PL decay of the D1 line from a piece of self-implanted Si was collected with the notch filter in place - the decay time of D1 has been reported to be less than 1520 ns at 9.3K. [11] Both techniques gave the same system response time of 10μs. The temperature was varied between 7.5K and 150K (beyond which the signal intensity became too low for the PL decay to be measured), and the average power density of the laser beam incident on the sample was 50mW cm^{-2}. PL spectra were measured using a slow North Coast Ge detector, dispersed with a spectrometer and the signal was analysed by standard lock-in

amplifier techniques. PL and the PL decay measurements were carried out without changing the path of the laser beam onto the sample, thus ensuring that both sets of data came from exactly the same volume of the sample.

For the electrical measurements, a variety of implant species was used to ascertain the effect of increasing ion mass on the nature of as-implanted defects. The starting material was n-type CZ silicon with a low resistivity. One sample was preserved untreated for reference purposes, whilst three were implanted at room temperature with silicon (Si:Si), ytterbium(Si:Yb) or erbium (Si:Er). All implants were carried out at room temperature after the predicted ion ranges had been calculated using the modelling tool Transport of Ions in Matter (TRIM). The implant energies were chosen so that implanted regions were encompassed within the depletion regions occurring at low reverse biases, in order that we could profile through the implanted region electrically. The doses were chosen to ensure that there was a minimum of carrier removal due to deep defect states after implantation. A comparison study of n-type Si, resistivity 2Ω-cm, which was irradiated with protons at 24GeV/c was carried out. This irradiation energy ensured that the protons passed right through the sample, leaving only residual damage. After implantation or irradiation, aluminium Ohmic contacts were evaporated on the rear face, and gold Schottky contacts on the front face. Table I summarises all the sample details, implanted ions and implantation conditions.

A high stability cryostat was employed for the LDLTS measurements [12]. This technique records the capacitance transient due to carrier emission at a fixed temperature and applies mathematical algorithms to extract the emission rates present in the transient. The choice of temperature is dictated by the original DLTS measurement, i.e. a temperature is chosen at which there is a peak in the DLTS spectrum. Several thousand capacitance transients were averaged,

which ensured that the signal-to-noise ratio was ≥ 1000:1, which is necessary to separate transients with closely spaced emission rates [12]. The transient was analysed and a plot of peak intensity as a function of emission rate produced. If the transient is truly exponential, only one peak is visible in the LDLTS spectrum, and the area under each sharp peak is proportional to the concentration of the deep level with that emission rate.

Results and Discussion: Optical Characterisation

Figure 1 shows the PL decay of the optically active sample 1 recorded at 1.54μm from two different areas of the sample. The dashed line shows PL decay from an area of the sample which has a greater proportion (amplitude) of fast decay component than the area shown as a solid line in the figure. Decay lifetimes were found by curve fitting to a two-exponential decay of the form

$$A_1 \exp\left(-\frac{t}{\tau_1}\right) + A_2 \exp\left(-\frac{t}{\tau_2}\right) \qquad (1)$$

where τ_1 is the decay time of the fast component and A_1 its amplitude at t=0; τ_2 and A_2 similarly describe the slow component. The values of the four variables were determined by a least mean squares routine. The fast lifetime marked on the figure was determined to be 148μs and the slower decay was found to be 827μs. A faster PL decay time is indicative of competition to the slower erbium luminescence, and it could be due to the Auger de-excitation, a back transfer process, an alternative as yet undefined route, or a combination of these.

Figure 2 shows the PL for the same two areas of sample 1. The narrower peak was collected from the area which exhibited less fast component in the decay, i.e. the decay had a smaller value of A in equation 1, and the broader peak was measured from the area with more fast component

(larger A). This latter spectrum exhibits a broadening on the low wavelength, high energy side, which is typical of D1-type luminescence lineshapes in dislocated Si. D1 and erbium emit light centred at approximately the same wavelength.

If the fast component of the decay is due to an Auger process involving free carriers, as has previously been reported, [13] then the temperature dependence of the decay time should follow the relationship

$$\tau = \frac{1}{1/\tau_0 + A\exp(-\varepsilon/2kT)}. \quad (2)$$

where τ is the decay at temperature T, A is a constant, and ε is the energy of the shallow donor or acceptor. Figure 3 shows data for the fast and slow decay times of sample 1 as a function of temperature. It is clear that the slow and fast components of the PL decay exhibit quite different behaviour. Moreover, the slow decay as a function of temperature is very similar to that reported in reference 13. The fast decay data cannot be fitted to equation 2, and therefore it is unlikely that the fast decay in this sample is due to an Auger process involving free carriers. Because of the shape of the PL spectra in Figure 2, it is suggested that the fast component is dislocation-related. Sobolev et al.[14] find the directly measured decay time for D1 in deliberately dislocated erbium-implanted silicon is 50μs, which is close that of the fast decays in this work.

After the PL experiments were complete, the sample was etched with the preferential etch Y3 [15] in order to reveal, by optical microscopy and SEM, any crystallographic defects present. Figure 4 shows an SEM image taken from an area of the sample with the greatest fast decay amplitude at 10K, as determined by equation 1. Small crystallographic defects can clearly be observed in this image. The area with the smallest amplitude of fast decay time showed no such

crystallographic defects, and these results support the suggestion that extended defect-related luminescence is present alongside the luminescence from the erbium.

Results and Discussion: Electrical Characterisation

We now examine whether precursors to this damage are present in the implanted Si before any annealing, and whether it can be detected. It is of most interest to examine the interstitial-rich region (discussed below) for clusters, as they would be precursors to end-of-range-loops or related damage. Some small clusters of interstitials have dangling bonds and therefore could possess a deep state in the band gap. As previously stated, this experimental procedure demanded a lower implant dose than sample 1, which needed to be optically active. The lower dose experiments are still valid however: because higher doses increase the damage introduction rate, it can be assumed that, should evidence of damage clusters be present, they will be more significant at higher doses, prior to anneal.

When ions are implanted into a semiconductor host, there is compelling evidence that the region between the peak and the surface is richest in vacancies, and the region after the peak towards the end of range is richest in interstitials [16]. The interstitials have the potential to cluster and form end-of-range or other extended defects during anneal, but it is not known experimentally whether small defect clusters are formed prior to an anneal, and whether they exhibit electrical activity. In this section we compare the properties of rare-earth implanted Si, with Si implanted with other ions and much lighter particles, to examine the differences. Figure 5 shows the DLTS spectra of Si implanted with protons, Si and Er. The spectrum from the Si implanted with Yb was virtually identical to the Er-implanted one, and is not shown for clarity. It is clear that the ratio of the peak height at approximately 235K to the peak height at 100K is changing, and Table

II shows this ratio for the Si-, proton-, Er- and Yb-implanted samples. The lighter particles produce a ratio below 5, whereas the heavier, rare earth ions produce a value two orders of magnitude greater than this. Careful inspection shows that this peak also changes to a lower temperature by about 10K in the case of the rare earth implant, and we return to this point later.

Because of these differences, we deduce that the overall effect of the heavier ion implant is primarily apparent in the feature at around 235K. The features in the DLTS spectra from the proton and, by association, Si, implanted Si are well known [17-19], and are listed in Table IIII. For some years it was thought that heavier ion implant damage was directly comparable to electron or proton irradiation damage, prior to anneal, but Figure 5 illustrates that this is not the case.

The reverse bias voltage employed in DLTS measurements can be chosen to investigate a particular depth behind the surface, which can be used for electrical profiling of deep states from the surface inwards. Its use is limited by the restrictions placed on knowing the depth accurately because of Debye tail effects. Nevertheless it can be employed for the characterisation of regions well separated from each other. Based on the tenet, described before, that there distinct vacancy- and interstitial-rich regions in ion-implanted samples, reverse bias voltages were chosen to capture data from each of these two regions. The DLTS spectra did not alter significantly between the two regions, and therefore they are not shown, but the LDLTS spectra were quite different. The LDLTS measurement temperature was set to that of the maximum of the large peak at around 235K, because of the assumption that this is where the differences lie in the heavy ion implanted samples.

Figure 6 shows the LDLTS of sample 2, low dose Er-implanted Si, before annealing. The measurement temperature was 225K and the experiments were carried out at two voltage ranges: a reverse bias of –2 V and fill pulse of –1 V which examined the vacancy-rich region, and a reverse bias of –5 V and fill pulse of –4 V which examined the interstitial-rich region. These values were obtained by a comparison of Capacitance -Voltage (C-V) data with simulations of the implant profile by TRIM. The vacancy-rich and interstitial-rich regions differ from each other, and also neither of the LDLTS spectra exhibit the two lines that would be expected for a point defect profile due to proton or electron irradiation, as described in Table III. If electrons or protons are implanted, one would see either one or two lines depending upon the doping, due to the singly charged divacancy, VV, and the dopant-vacancy pair, (VP in this case), if the background doping were high enough. [17] Figure 6 shows more than two components in the capacitance transient in both cases: three from the interstitial-rich region and five from the vacancy-rich region. Samples 3 and 4 also showed the same trend of five emission rates in the vacancy-rich region, simplifying to three in the interstitial-rich region. Repeated experiments over several days showed that the results were reproducible, and all emission rates increased with temperature, as should be the case for emission from deep states. However, because the capacitance transient displayed so many components, the trap concentration of each individual deep level was small. Therefore, the signal to noise ratio was quite low, and Arrhenius plots to obtain the activation energies were not possible. Sample 5, the proton-irradiated silicon, did not exhibit a complex structure in the LDLTS spectra recorded at this temperature.

To further confirm that the peak at around 230K in the rare earth implanted Si is not due to the simple VV and V-dopant defects seen in sample 5, Figure 7 shows how the temperature of the maximum of the DLTS emission varies with anneal temperature for sample 2, Yb-implanted Si.. All anneals were for 10 minutes. Also shown for reference are the maxima of the peaks in the Er-

implanted Si and proton irradiated samples, at zero anneal time, (slightly offset for clarity). It can be seen that the peaks in samples 1 and 2 are in the same place at zero anneal, but the Si- and proton-irradiated samples exhibit peak maxima with higher temperatures. As the anneal temperature is increased beyond 200K, the emission temperature approaches that of samples 4 and 5. Similar behaviour is observed for sample 2. There are two possible reasons for this. Either the new defects in samples 2 and 3 are annealing out, leaving the more typical point defects found in light ion damage, or the electrical activity of these defects begins to decrease above 200K. Therefore, either the defects are dissociating, or growing by Ostwald ripening into non-electrically active defects, for example I4 or I8, as previously modelled by Cowern et al [8]. If the former suggestion is true, released interstitials may then assist the development of end-of-range loops. If the latter case holds true, the Ostwald ripening of the small clusters leads to the formation of the end-of-range loops. In reality, both processes will be occurring in parallel – some clusters will feed the growth of other clusters at their own expense. It is likely that the reduction in the peak height is due to a combination of the two processes, as both lead to non-electrically active defect states.

It remains to determine whether this new damage product has point- or extended-defect like characteristics. We again focus on the interstitial-rich region, as this is from where end-of-range loops will acquire the interstitials needed to enable their growth. A sensitive test for the presence of extended defects, even those too small in size or number to be detected by electron microscopy, is to examine their capture kinetics in the DLTS experiments. The majority capture cross section σ_n is given by [20]

$$\ln\left[\frac{\Delta C_\infty - \Delta C_t}{\Delta C_\infty}\right] = \sigma_n V_{th} n t_p \qquad (3)$$

where t_p is the pulse length, n is the majority carrier population; V_{th} is the thermal velocity, ΔC_∞ is the equilibrium capacitance value and ΔC_t is the capacitance at time t. In the DLTS technique the pulse length is normally chosen so that the deep levels are totally filled. However, trap filling can be influenced by changing any one of the variable parameters in equation 1, and the simplest way to do this is to change t. This is achieved by shortening the pulse length, and incomplete trap filling then occurs. According to Equation 3, the majority capture cross-section should obey a linear dependence on the logarithm of a combination of capacitance terms. Deviation from this relationship provides a sensitive test for the presence of extended defects. As extended defects capture more carriers, they become progressively more charged, and exhibit increasing Coulombic repulsion; the repulsive force reduces subsequent carrier capture at the defect. The capture cross-section therefore becomes dependent upon the amount of charge already captured at the defect(s), and become times dependent.

The simplest way to oserve this is to plot the results in accordance with equation 3, and test for deviations from non-linearity. There are other reasons this can occur, but generally they only occur in very specialised circumstances. [21] Figure 8 shows such a plot for Er-implanted Si, sample 2, and the proton-irradiated sample 5, which should contain no extended defects as the protons pass straight through the sample. The measurements were carried out at 235K, the peak of interest, and the fill pulse was varied from 1000ns to 1ms. The voltage for the measurements was a reverse bias of –5V and fill pulse of –4V, which samples the interstitial-rich region in the Er-implanted sample. The proton data, shown as solid circles, has been fit to equation (3), and an excellent fit is obtained, as shown by the solid line through the data points. The erbium data, shown by crosses, cannot be fitted to this equation, because the gradient of the data reduces progressively as the DLTS fill pulse duration is increased. The capture cross section is proportional to the slope of this data (equation (3)) and therefore this confirms that the apparent

capture cross section, if it could be measured, is decreasing with fill pulse time. This is indicative of an energy state(s) becoming more repulsive to further capture as the experimental time progresses, i.e. the defect is charging up. This is classic dislocation behaviour [22] it was also observed in our Si- and Yb-implanted samples. A potential barrier is built up around the extended defect as it becomes increasingly negatively charged, as it continues to trap electrons. This confirms that the peak at 235K in the ion implanted samples contains defects which do not exhibit simple point defect-like behaviour, and it is deduced that this DLTS peak arises from small extended defects, maybe containing just a few interstitials, immediately after implant. This effect is, naturally, independent of the ion species.

Conclusions

Detailed electrical studies by high resolution Laplace Deep Level Transient Spectroscopy of Si samples implanted with a variety of implanted ions, including Er, show that there are small, electrically active extended defects present in the interstitial-rich region immediately after implant. Capture cross section measurements confirm that these new defects are not point defects. Annealing studies show that the electrical activity of these defects begins to decrease above 200K. Either the defects are dissociating, or growing by Ostwald ripening into non-electrically active defects, for example I4 or I8, as previously modelled by Cowern et al. If the former, interstitials will be released from them to assist the development of end of range loops. If the latter, Ostwald ripening causes these defects to grow and form the end-of-range damage. It is likely that the reduction in the peak height is due to a combination of the two processes, as both lead to non-electrically active defect states. Only the use of LDLTS has enabled this identification, as conventional DLTS shows very similar signatures after implant that cannot be

separated into separate peaks for closely spaced energy states in the band gap. The defects are observed in all ion implanted samples, not just the Er-implanted sample.

Photoluminescence, PL decay measurements, and microscopy studies show a direct correlation between the PL lifetimes and the presence of small end-of-range extended defects in the Er-implanted sample. The higher the defect density, the larger the fast lifetime component in the PL decay. It has been shown that this is caused by emission from the well-known dislocation line D1 which originates from the end-of-range damage..

It is therefore concluded that there can be competition to the radiative efficiency in rare-earth implanted Si that is due to the implantation process and is not specific to Er. This is in addition to any back-transfer or Auger processes thought to be responsible for the reduced efficiency of the Er PL at higher temperatures.

Acknowledgments

We would like to acknowledge Dr P Dawson, Dr I Hawkins and Dr N Abdulgader for help with the experiments. K Vernon-Parry would like to acknowledge the UK Engineering and Physical Sciences Research Council for an Advanced Research Fellowship.

References

[1] P. G. Kik and A. Polman, in L. Pavesi et al (Eds), Towards the First Silicon Laser, Kluwer Academic Publishers, 2003, p.383

[2] C. E. Chryssou, A. J. Kenyon, T. S. Iwayama, C. W. Pitt, and D. E. Hole, Appl. Phys. Lett., 75 (1999) 2011

[3] G. Franzo, V. Vinciguerra, and F. Priolo, Appl. Phys. A, 69 (1999) 3

[4] V. Touboltsev and P. Jalkanen, J. Appl. Phys., 97 (2005) 013526

[5] N.E.B Cowern, B. Colombeau, J. Benson, A. J. Smith, W. Lerch, S. Paul, T. Graf, F. Cristiano, X. Hebras, D. Bolze, Appl. Phys. Lett., 86 (2005) 101905

[6] M. Benzohra, F. Olivie, M. Idrissi-Benzohra, K. Ketata, and M. Ketata, Nucl. Instr. Meth. Phys. B, 187 (2002) 201

[7] Yu. Shreter, J.H. Evans, B. Hamilton, A. R. Peaker, C. Hill, D. R. Boys, C. D. Meekison and G. R. Booker, Appl. Surf. Sci., 63 (1993) 227

[8] N. E. B. Cowern, G. Mannino, P. A. Stolk, F. Roozeboom, H. G. A. Huizing, J. G. M. van Berkum, F. Cristiano, A. Claverie, and M. Jaraiz, Phys. Rev. Lett., 82 (1999) 4460

[9] J. Michel, J. L. Benton, R. F. Ferrante, D. C. Jacobson, D. J. Eaglesham, E. A. Fitzgerald, Y-H Xie, J. M. Poate and L. C. Kimmerling J. Appl. Phys., 70 (1991) 2672

[10] S. Coffa, G. Franzò, F. Priolo, A. Polman and R. Serna, Phys. Rev., B 49 (1994) 16313

[11] S. Fukatsu, Y. Mera, M. Inoue, K. Maeda, H. Akiyama, and H. Sakaki, Appl. Phys. Lett., 68, (1996) 1889

[12] L. Dobaczewski, P. Kaczor, I.D. Hawkins and A.R. Peaker, J. Appl. Phys., 76 (1994) 194

[13] F. Priolo, G. Franzò, S. Coffa, and A. Carnera, Phys. Rev. B, 57 (1998) 4443

[14] N. A. Sobolev, O. B. Gusev, E. I. Shek, V. I. Vdovin, T. G. Yugova, and A. M. Emel'yanov, Appl. Phys. Lett., 72 (1998) 3326

[15] K. H. Yang. J. Electrochem. Soc. 131 (1984) 1140

[16] P. Pellegrino, P. Leveque, J. Wong-Leung, C. Jagadish and B. G. Svensson, Appl. Phys. Lett. **78**, 3442 (2001)

[17] G.D. Watkins and J.W. Corbett, Phys. Rev. 138, (1965) A543

[18] M.T Asom, J.L. Benton, R. Sauer, and L.C. Kimerling, Appl. Phys. Lett. 51, (1987) 256

19] J. Lalita, B.G. Svensson, C. Jagadish, and A. Hallen, Nucl. Instr. and Meth. B 127/128, (1997) 69

[20] D.V. Lang, J. Appl. Phys., 45, (1974) 3023

[21] N. Abdelgader and J. H. Evans-Freeman, J. Appl. Phys., 93 (2003) 5118

[22] P. R. Wilshaw and G. R. Booker, in Proceedings of the Royal Microscopical Society Conference, Eds. A. G. Cullis and D. B. Holt, Inst. Phys Conf Ser. 76 (1985) 329

Table I Sample Details

sample name	Starting resistivity (Ω -cm)	implanted ion	dose (cm^{-2})	implant energy (MeV)	carrier concentration directly after implantation (cm^{-3})
1	0.8	Er O	$5x10^{13}$ 0.45 0.30 0.20 0.14 0.90 0.70	1 $3.2 x10^{14}$ $2.0 x10^{14}$ $1.4 x10^{14}$ $1.1 x10^{14}$ $5.0 x10^{14}$ $1.0x10^{14}$	not measurable
2	2-4	Er	$1 x 10^{9}$	2	$2.7 x 10^{15}$
3	0.85	Yb	$3 x 10^{10}$	4	$2.0 x 10^{15}$
4	2-4	Si	$1 x 10^{9}$	0.8	$2.3 x 10^{15}$
5	2	protons	$1 x 10^{11}$	24GeV/c	$6.0 x 10^{15}$

Table II Ratios of DLTS peaks

Maximum trap concentration (cm^{-3})	Temp of DLTS peak (K)	Ratio of high T peak height to low T peak height	Implanted atom/particle
$2.14x10^{14}$ $9.05x10^{11}$	223 100	236	Er
$2.14x10^{14}$ $4.45x10^{11}$	225 95	480	Yb
$3.24x10^{13}$ $2.34x10^{13}$	235 95	1.38	Si
$2.13x10^{14}$ $1.70x10^{13}$	230 95	1.24	protons

Table III Common irradiation defects in proton or electron irradiated Si

approximate DLTS peak temperature at rate window $200s^{-1}$ (K)	Assignment of defect	activation energy E_C - E_t (meV)
70	carbon-substitutional+Si-interstitial complex	
95	vacancy-oxygen, VO	170
130	doubly-charged di-vacancy, VV	225
175	VOH	320
240	VV and dopant-vacancy (usually VP) defects with very close energies	450
280	V_2H?	>450

Figure Captions

Figure 1   PL decay measured at 1.54µm for two areas of sample 1. The dashed line (----) shows PL decay which has a greater proportion of fast decay component than the area shown as a solid line (______).

Figure 2. Two PL spectra from the same areas on sample 1 as in Figure 1, measured at 7.5K. The dashed line (----) is a spectrum measured from an area with a greater proportion of fast PL decay component than the area whose spectrum is shown as a solid line (______)

Figure 3. The fast (◊) and slow (+) components of the PL decay of sample 1, as a function of temperature. The data corresponds to the dashed line in figure 1, and was taken from the same area.

Figure 4. Scanning electron microscopy image of sample 1, the optically active Er-implanted sample, after annealing and etching as described in the text. This is the area that gave rise to the broader PL spectrum indicated with a dashed line in Figure 2.

Figure 5. DLTS of samples 2 (Er implanted), 4 (Si implanted) and 5 (proton irradiated).

Figure 6. LDLTS of sample 2, low dose Er implanted Si, before annealing. The measurement temperature was 225K and the experiments were carried out at two voltage ranges: a reverse bias of –2 V and fill pulse of –1 V which samples the vacancy-rich region, and a reverse bias of –5 V and fill pulse of –4 V which samples the interstitial-rich region.

Figure 7. DLTS peak temperature of new defect peak at around 225K (zero anneal) as a function of anneal time for sample 3, Yb implanted. Samples 2,4,5 at zero anneal are shown for comparison.

Figure 8. The capacitance transient height plotted as a function of DLTS fill pulse duration, in accordance with equation 3, for sample 5, irradiated with protons (●) and sample 2, low dose Er-implanted Si, (+).

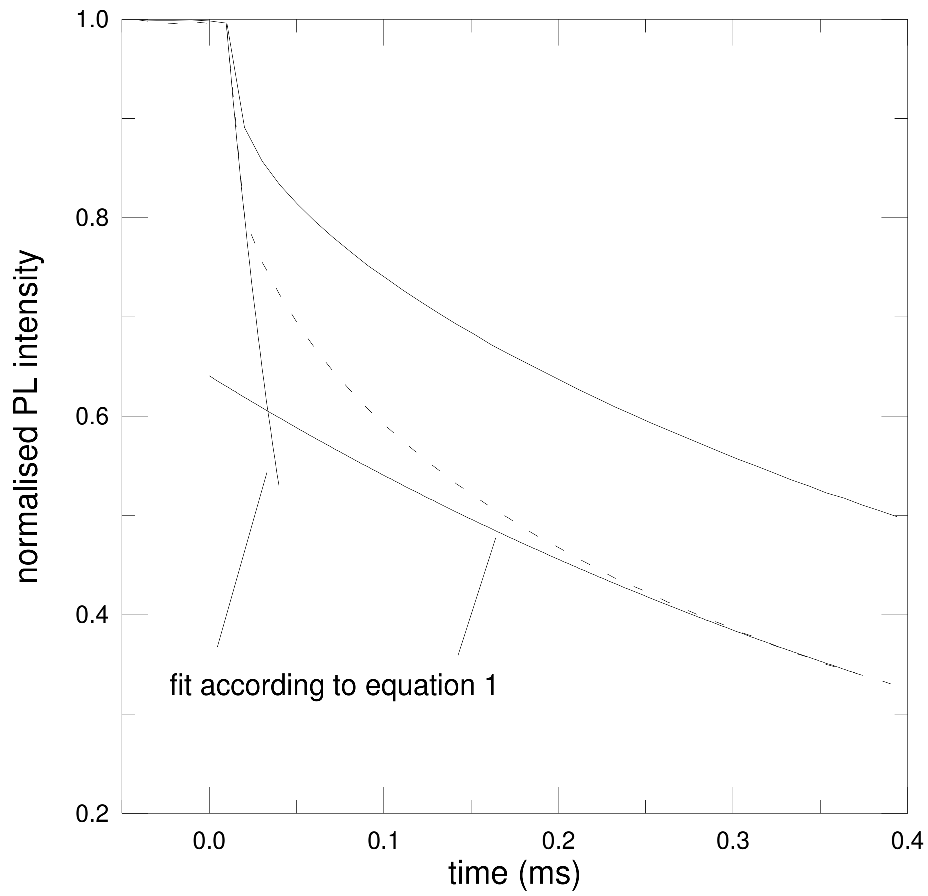

Figure 1

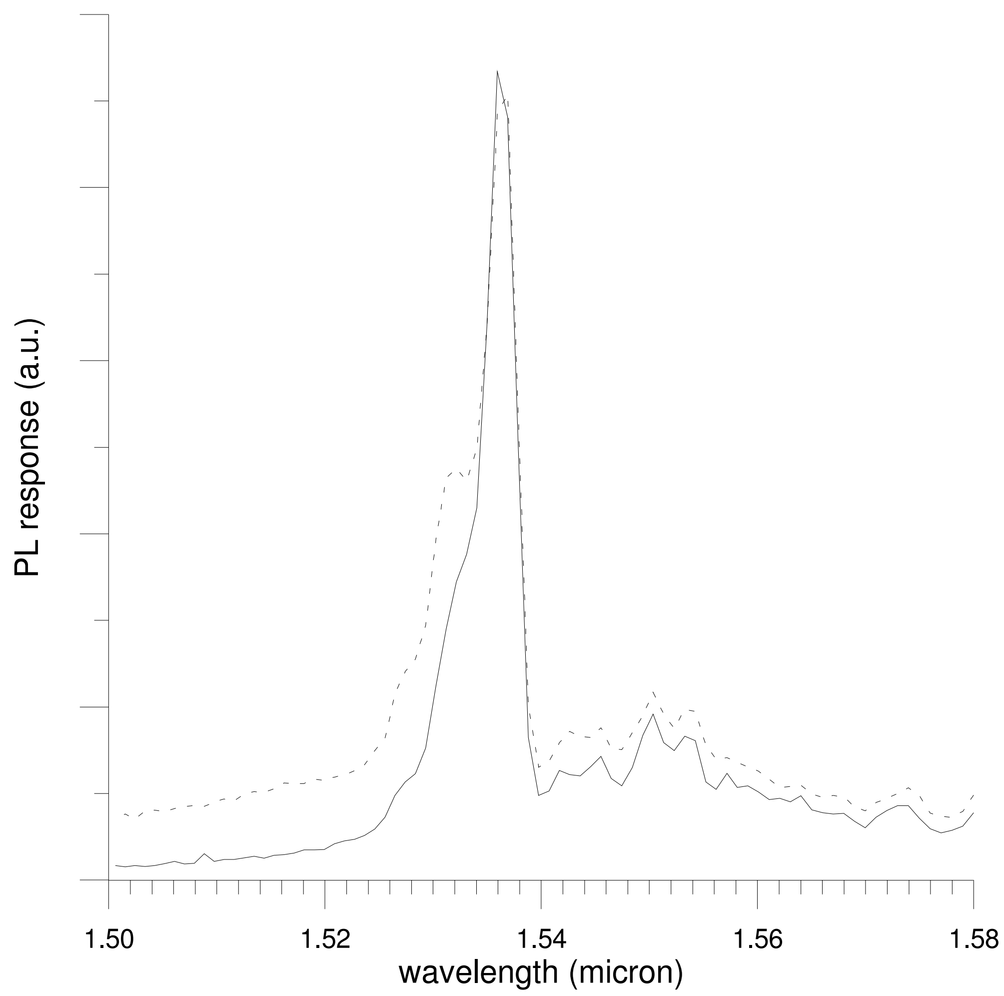

Figure 2

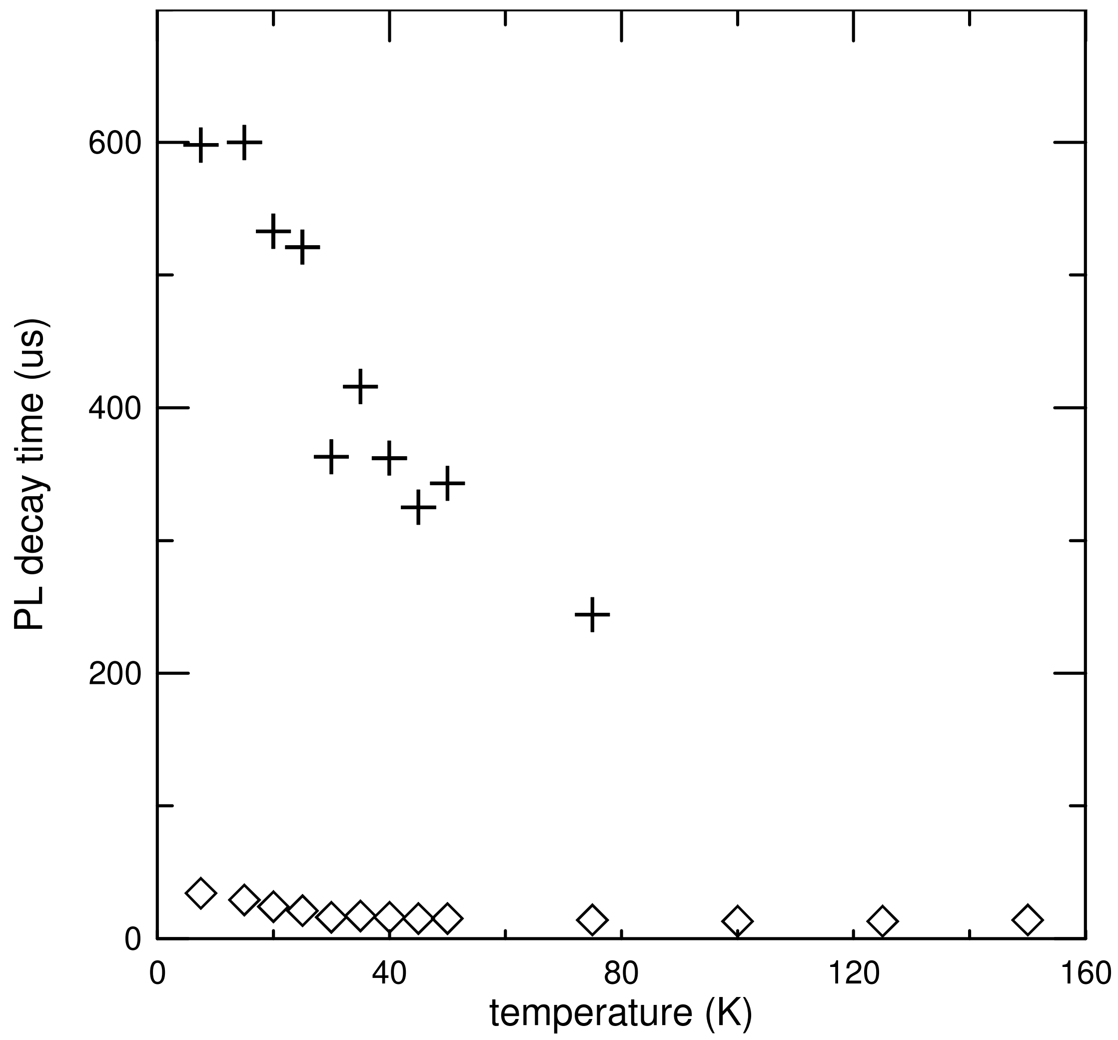

Figure 3

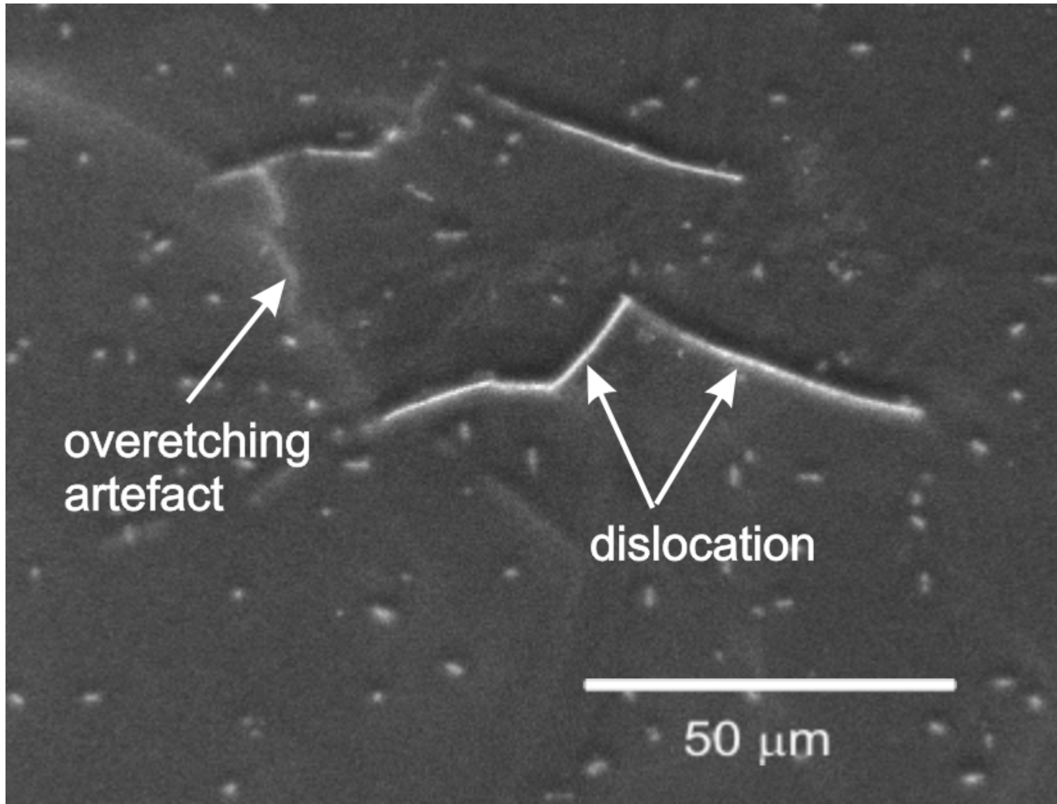

Figure 4

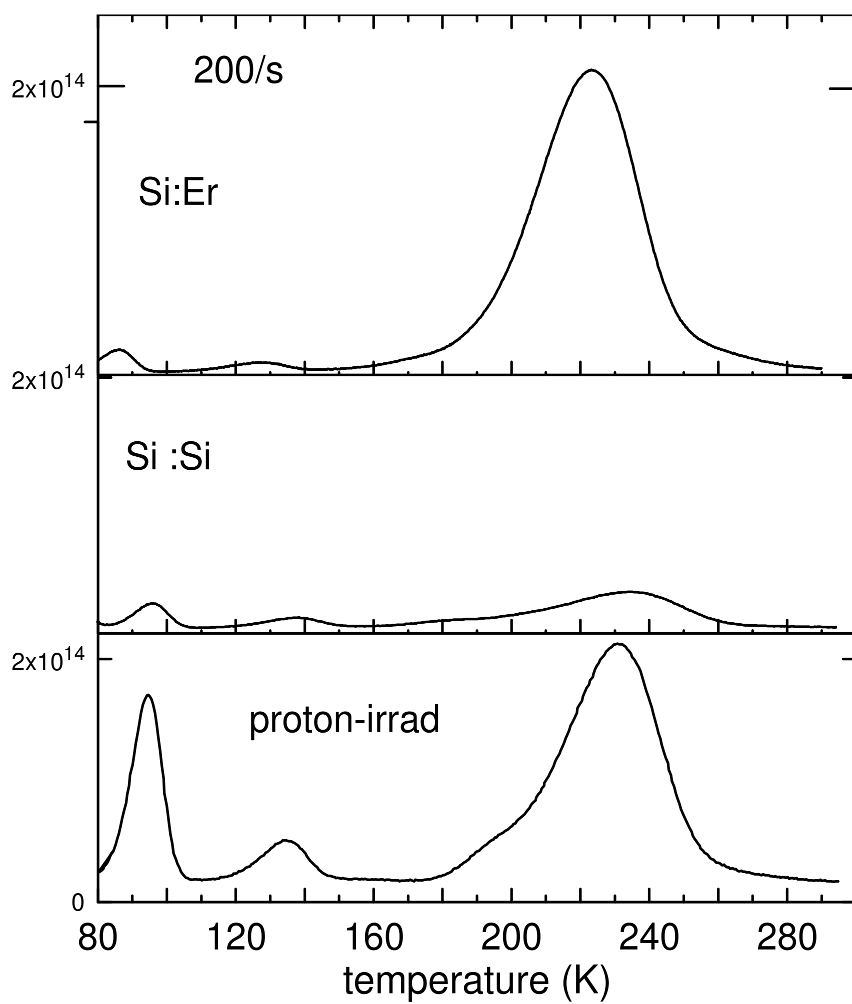

Figure 5

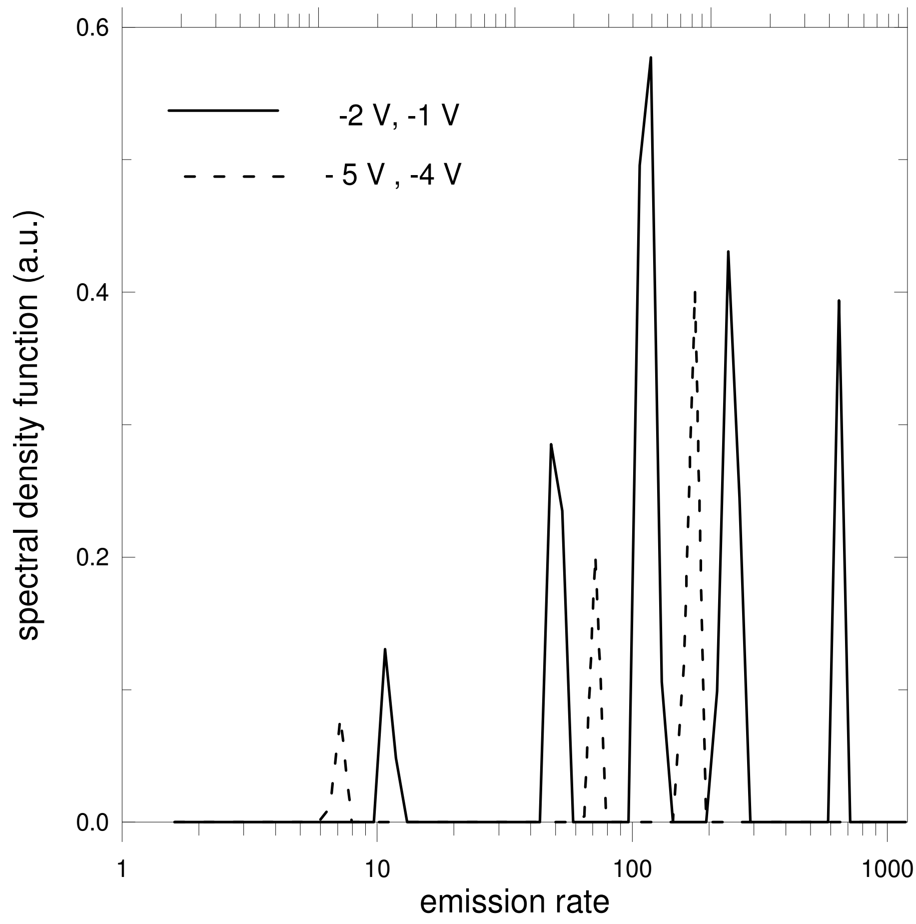

Figure 6

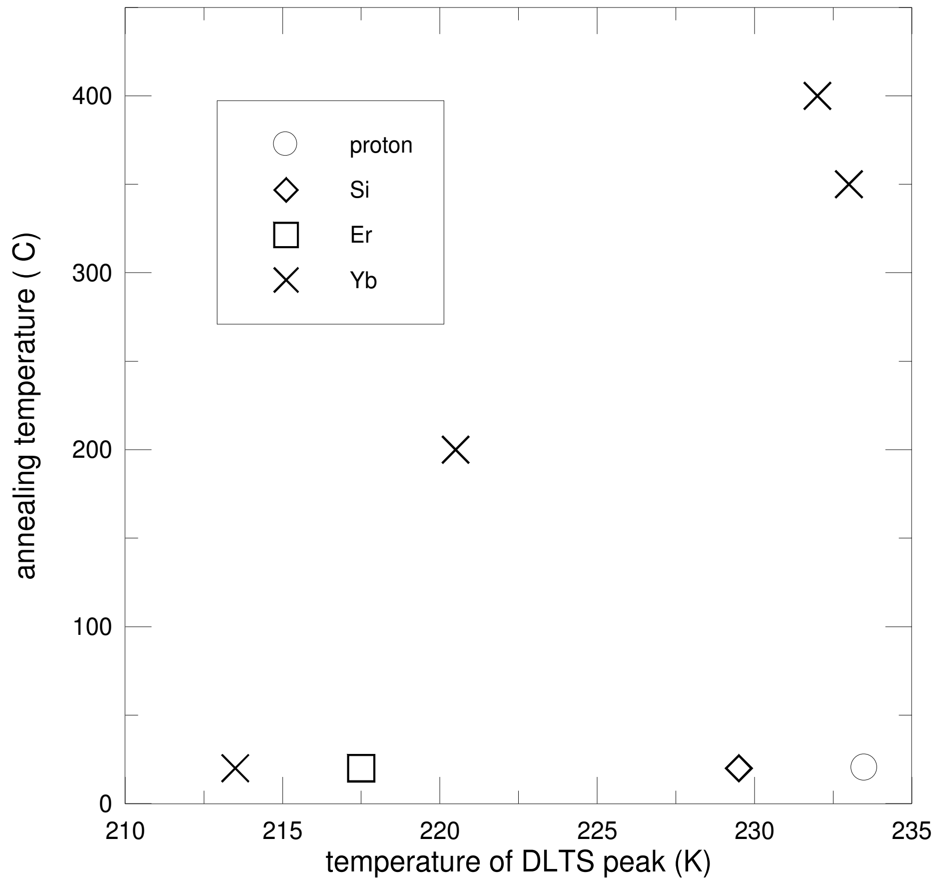

Figure 7

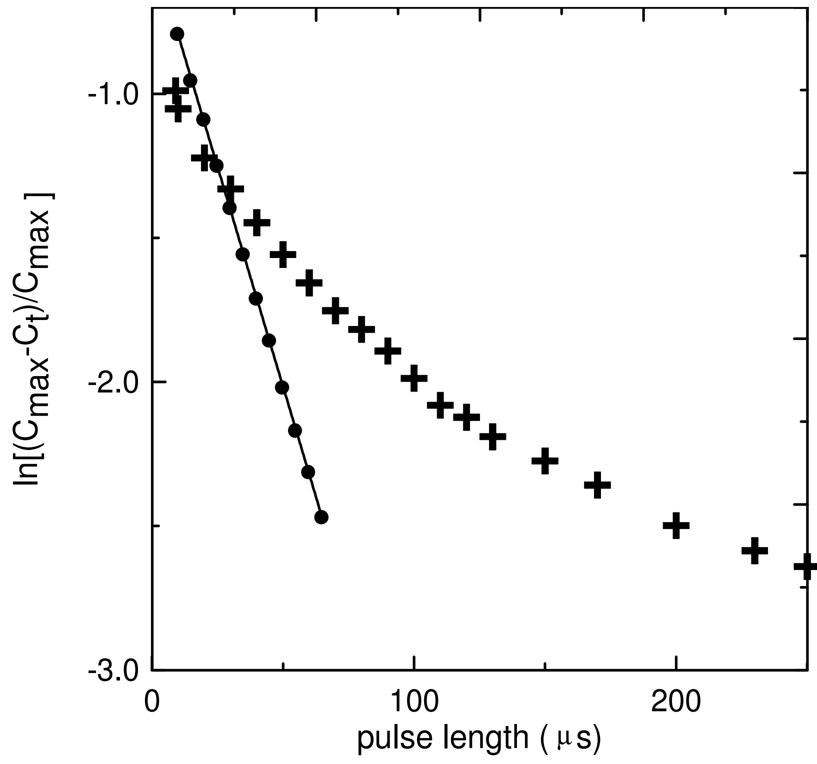

Figure 8